Facile Control of Liquid-Rope Coiling With Tunable Electric Field Configuration

Jingxuan Tian,[1] Jingmei Li,[1,2] Alban Sauret,[3] Tiantian Kong,[4] Xiaoxiao Wu,[5] Yongjie Lu,[1] and Ho Cheung Shum[1,2,*]

[1]*Department of Mechanical Engineering, The University of Hong Kong, Pokfulam Road, Hong Kong, China*
[2]*The University of Hong Kong-Shenzhen Institute for Research and Innovation (HKU-SIRI), Shenzhen 518000, China*
[3]*Department of Mechanical Engineering, University of California, Santa Barbara, California 93106-5070, USA*
[4]*Department of Biomedical Engineering, School of Medicine, Shenzhen University, Shenzhen 518060, China*
[5]*Department of Physics, The Hong Kong University of Science and Technology, Clear Water Bay, Kowloon, Hong Kong, China*

(Received 6 February 2019; revised manuscript received 8 April 2019; published 18 July 2019)

Liquid-rope coiling occurs when a thin jet of viscous fluid falls from a sufficient height onto a rigid substrate. Coiling can also be induced by an electric field, and this precise control over coiling has inspired alternative applications in direct writing, such as the printing of nano-objects and the mixing of viscous fluids. However, the physical mechanism of electric field-assisted coiling remains inadequately understood, challenging the optimization of the design of printing setups. We identify the subtle role of the electric field profile on the jet morphology and the onset of coiling, especially the height, by modifying the electrode configuration for controlling an electrified jet. Based on our finding, we demonstrate that the viscous coiling effect can be either induced or suppressed by changing the configuration of the electrodes, which tunes the electric field profile. The exquisite control of the coiling of viscous fluids can enhance applications that require dispensing of viscous liquids and on-demand direct writing for a wide range of working conditions and various printed patterns.

DOI: 10.1103/PhysRevApplied.12.014034

I. INTRODUCTION

Electrified jets are of great potential to benefit the emerging rapid, high-resolution printing [1–4]. Electric stress can accelerate and stretch a liquid jet [5], thus significantly reducing the jet diameter, saving the technical complexities involved when extruding viscous liquid from tiny nozzles. As an electric field can suppress the Rayleigh-Plateau instability completely for a viscous jet in air [6–8], the liquid thread can be deposited onto a substrate continuously without breaking up to achieve a diameter of a filament hundreds of times smaller than that of the nozzle size [9]. A charged jet can manifest a coiling behavior in the presence of an electric field under appropriate operating conditions [10,11], because it is an intrinsic tendency for a significantly thinned and accelerated liquid thread to buckle, bend, and coil, which is commonly termed as liquid-rope coiling [12,13], which contains rich dynamics [14–16] and applications [17–20]. Unlike the spontaneous coiling that can only happen above a critical dispensing height, which allows the jet to get sufficiently thinned and accelerated [21–23], the minimum dispensing distance to trigger coiling for a charged jet and the result jet diameter can be significantly scaled down compared to an uncharged jet. This approach has been exploited to print patterns of fibers with improved resolution to as fine as hundreds of nanometers [24] or to handle viscous fluids, which are usually cumbersome to manipulate due to their sticky and thick natures [10]. Besides electric coiling, other techniques such as electrospinning [5,25–27] or electrospray [28,30], where tiny liquid threads and droplets are formed under electric charging, can also be induced under appropriate operating conditions for material synthesis or engineering of functional structures. Given the rich dynamics of electrified jets, a comprehensive understanding and control over electrified jets are critical in designing strategies to achieve different electrically induced liquid structures for target applications. While the operating parameters, such as applied voltages and liquid flow rates are widely studied [31–36], the configuration of the electrical charging setup remains inadequately investigated, despite its rich underlying physics. In practice, a tip-to-plate configuration of electrodes is commonly adopted to charge liquid jets, and the corresponding analysis usually assumes the electric field to be vertical and uniform for simplicity [10,11,24], typically that of a plate-to-plate electrode configuration. While this simplified assumption is valid for some situations, it fails to distinguish

*ashum@hku.hk

between jet dynamics observed under different electrode configurations. Hence a more sophisticated explanation to describe the electrified jet is critical. Besides inducing jet coiling, there is also a need to suppress it, especially in applications where coiling undermines the quality of fiber-based products. For example, the compromised toughness of glass plates due to the irregularities that arise from coiling of molten glass during fabrication remains challenging to address [37]. In short, understanding the mechanism of electrified jets and the ability to manipulate the coiling behavior on demand is highly desired for engineering printed structures.

In this work, we take the shape of the electric field into account when characterizing the electric field. We investigate the jet morphology and dynamics while tuning the electric field profile systematically by changing the electrode configuration from a tip-to-plate to a plate-to-plate setup. We demonstrate that the onset height of coiling substantially differs as the electric field profile changes. We further identify its role in shaping the jet morphology, which, in turn, influences the onset of the coiling effect. Based on these results, we have proposed an explanation, which can account for the experimental observations that cannot be supported by previous simplified models. To confirm our understanding, we demonstrate the control over the triggering and suppression of coiling simply by changing the electrode configurations. Hence, our work introduces electrode configuration as an alternative degree of freedom for controlling electrified jets. The robustness of our finding is confirmed by printing tunable porosity patterns through switching the coiling effect on and off on demand. Our work enriches the physical picture of an electrified liquid thread and provides an effective solution for controlling viscous liquid jets for emerging printing applications.

II. EXPERIMENTAL METHODS

A. Electric field

A common experimental setup used to electrify liquid jets is composed of a metallic nozzle connected to a ground substrate, forming a tip-to-plate configuration as shown in Fig. 1(a) [26,27]. In this study, we consider an alternative version of the experimental setup where the

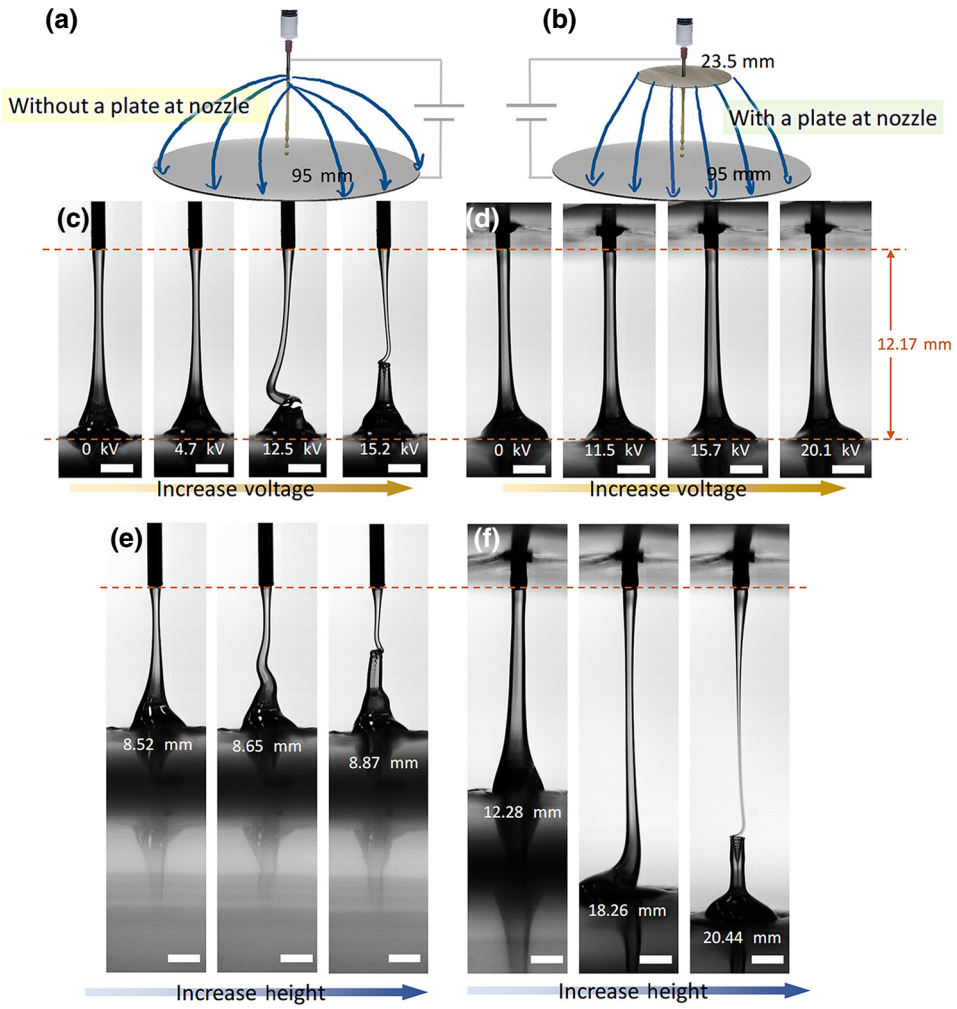

FIG. 1. Viscous jet coiling under electric field schematics of experimental setup (a) without a plate electrode at the nozzle and (b) with a plate electrode at the nozzle. Schematic electric field shape is shown by blue lines. When the applied voltage is increased from 0 to 20 kV while keeping the dispensing height constant, (c) the jet under a tip-to-plate configuration starts to coil while (d) the jet under plate-to-plate configuration remains stable. If the dispensing height is gradually increased while the applied voltage is kept at 5 kV, the viscous jet in the tip-to-plate configuration (e) starts to coil at a smaller height than the plate-to-plate configuration (f). Scale bars are 2 mm. Flow rate is 5 ml/h for all 4 cases.

top needle is surrounded by a metallic plate parallel to the bottom plate, as shown in Fig. 1(b). This plate-to-plate electrode configuration with an adjustable diameter of the top electrode enables the tunability in the distribution of the electric field, a feature not possible with a needle electrode only. We use circular-shaped aluminum plates of different diameters as top and bottom electrodes to ensure an axisymmetric distribution of the electric field. The diameters of the top electrodes are 5.5, 8, 13.5, 15, 18, 23.5, 29, 36, and 45 mm, while the diameters of the bottom electrodes are 30, 35, 40, 60, and 95 mm. The thickness of both plates is 0.5 mm. An electric field is imposed by connecting a direct current (dc) power source (Dongwen High-voltage Power Source Ltd., Tianjin, China) to the top and bottom electrodes. If the top and bottom electrodes are large enough and have similar diameters, the electric field lines are expected to be nearly parallel as profiled in the center region between the electrodes. In contrast, the common tip-to-plate experimental configuration of electrodes leads to diverging electric field lines.

B. Infusion

In experiments with electric fields, we use the same viscous fluid: lecithin from soya bean (Soy Lecithin, Wing Hing Chemical Company Ltd., Hong Kong). The fluid has a density $\rho = 1.045$ g/cm^3, a surface tension $\gamma \approx 30$ mN/m as measured by a pendant drop method [38], and a dynamic viscosity $\mu = 20$ Pa·s measured with a rheometer (Anton Paar, MCR310) with a measuring cone CP-25, a dielectric permittivity of approximately 23, and a conductivity of O(10^{-9}) S/m [10], and is regarded as a leaky dielectric fluid [39]. In the experiments without electric fields, silicone oils (Sigma-Aldrich, USA) of different viscosities are used. The fluid is loaded into a glass syringe (SGE Analytical Science, Australia) that is mounted onto a syringe pump (LSP01-2A, Longer Pump, Hebei, China), and a nozzle of 0.6-mm inner diameter is used for all experiments. The flow rate is 3–17 ml/h for all experiments. For electric field experiments in Figs. 1 and 2, the flow rate is 5 ml/h. In Fig. 4, the flow rate for nonelectrified jets varies for different fluids: 5–12 ml/h for lecithin, 9–17 ml/h for 10,000 cSt silicone oil, and 2–3 ml/h for 60,000 cSt silicone oil. For electrified jets, the flow rate is 3 ml/h. The flow rate we use in the printing application is 15 ml/h.

C. Data acquisition and experimental protocol

The dynamics of the jet is recorded using a high-speed camera (FASTCAM SA4, Photron, USA). The electrode-to-electrode distance is tuned by using a mechanical stage with a typical step resolution of 0.5 mm. For each dispensing height, the applied voltage to charge the viscous jet is gradually increased from 0 V to a threshold value where the jet gets straight and connects the two electrodes, or starts to coil, typically around 10–20 kV, depending on experimental parameters. We define the critical height, h_c, as the height below which no coiling of the jet is observed under any applied voltage. Above h_c, we observe the coiling of the jet when the voltage is increased to a sufficiently large value. More experimental details can be found in Sec. VI of Supplemental Material [40].

III. RESULTS

The tip-to-plate configuration of electrodes is commonly used for electric field-assisted coiling, and the resultant electric field is assumed to be vertical and uniform, which is typical for a plate-to-plate electrode configuration. However, our experiments suggest that these two configurations of electrodes cannot be taken as equivalent in terms of onset condition of coiling. Intriguingly, a jet that coils under a certain height and applied voltage [Fig. 1(c)] under tip-to-plate configuration will stop coiling if we attach a large aluminum plate to the nozzle and leave all other conditions fixed, as shown in Fig. 1(d). The additional metallic plate at the nozzle modifies the electric field profile and changes the dynamic behaviors of the viscous jet.

One explanation of this difference is that the strength of the electric field at sharp edges is often stronger than at blunt surfaces under the same applied voltage because the curvature is larger and the electric field lines that are perpendicular to the surface are denser. As such, the decrease in electric field strength E under the same applied voltage U could suppress coiling. To evaluate whether the disappearance of the coiling is due to a reduction of the electric field strength under the same height, we simulate the field strength at a selected point near the nozzle. The results indicate that when $U = 5$ kV, the field strength for tip-to-plate configuration is one magnitude larger than that for a plate-to-plate configuration case and will remain significantly larger until the applied voltage for the plate-to-plate case is increased up to 20 kV (see Sec. I of Supplemental Material [40] for simulations). Experimentally, a coiling jet at $U = 5$ kV in tip-to-plate configuration stops coiling when we attach the top plate electrode to the needle [Fig. 1(c)]. Then we increase the voltage to 20 kV and above, where the field strength has become comparable to that of a tip-to-plate configuration under 5 kV, according to simulation. However, the jet remains stable without coiling [Fig. 1(d)]. Therefore, the difference in field strength between plate-to-plate and tip-to-plate electrodes cannot explain the different dynamics of electrified jets.

To investigate whether the coiling will occur under the plate-to-plate configuration, we increase the dispensing height under a fixed voltage of 5 kV. The critical height that triggers the onset of coiling is about 20 mm under a plate-to-plate configuration [Fig. 1(f)], while the height is 12 mm under the tip-to-plate configuration [Fig. 1(e)]. This suggests that the critical height h_c for the onset of electrified coiling of a tip-to-plate setup differs substantially as

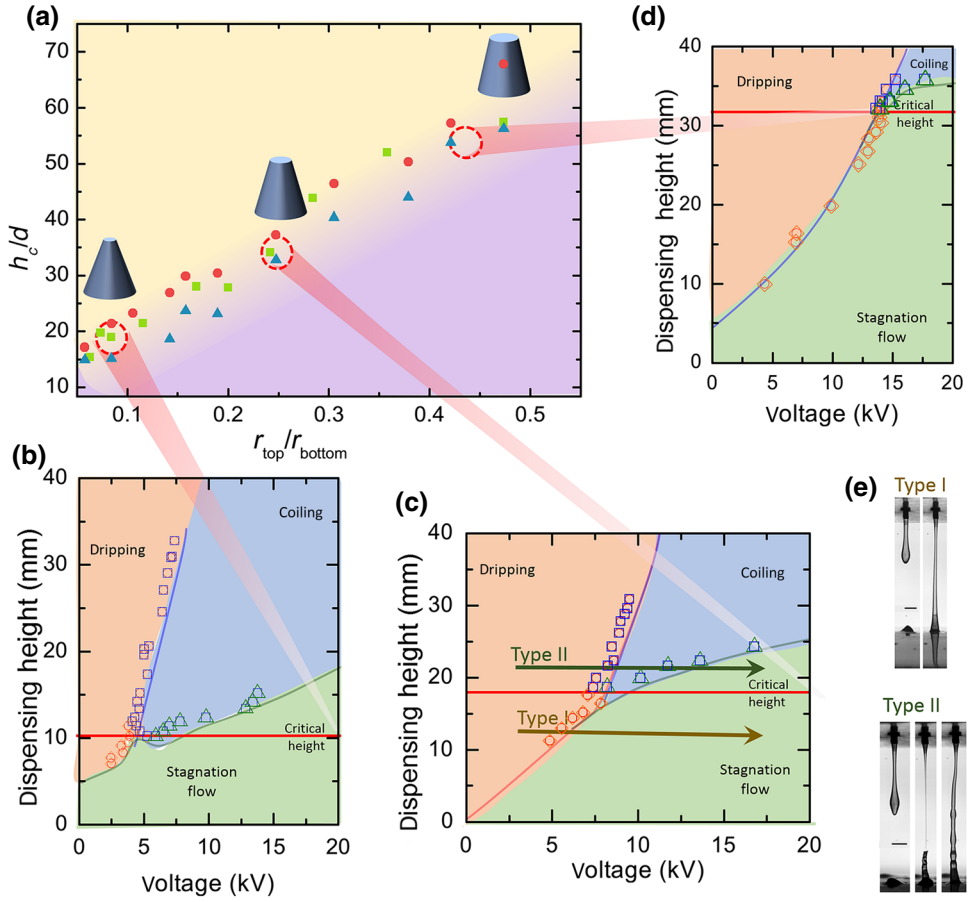

FIG. 2. Morphology diagram of the liquid jet under different heights (a) the normalized critical height h_c/d measured experimentally for different r_{top}/r_{bottom}. In this diagram, the yellow region indicates the coiling regime and the purple region is the noncoiling regime. Red circles, green squares, and blue triangles represent experiments with different sets of the top electrode and fixed bottom electrode. Results observed when the diameter of the bottom electrode is varied while keeping that of the top electrode constant can be found in the Supplemental Material, Sec. II [40]. Blue truncated cones are schematic shapes of electric field of their neighboring data. (b-d) Jet behavior as a function of the height and voltage for three different r_{top}/r_{bottom}: (b) 0.08, (c) 0.25, and (d) 0.42. The red line denotes the critical height, which represents the height below which the jet transitions from dripping to stable jet, and above which the jet transitions from dripping, to coiling, and finally to stable jet as the applied voltage increases. (e) Type I transition: dripping to stagnation flow; type II transition: dripping to coiling to stagnation flow. The flow rate is 5 ml/h.

we use a finite circular plate as the top electrode to form a plate-to-plate configuration.

To systematically study the effect of electrode configuration on the coiling behaviors, we measure the height and the voltage at the onset of the coiling for various combinations of top and bottom electrode radii. We denote the ratio of the top to bottom electrode radii as r_{top}/r_{bottom} and show the normalized critical height h_c/d as a function of it in Fig. 2(a) (See Supplemental Material [40] for critical height as a function of E_n/E_t). We can identify a clear increasing trend of h_c as r_{top}/r_{bottom} increases. The smaller the top electrode is and the more conical the field is, the smaller the critical height for coiling. Specifically, for each configuration, as the dispensing height or voltage is gradually increased, we observe the dynamic behaviors successively and categorize them as (i) a dripping jet, which corresponds to the state where the jet breaks up before reaching the substrate and does not form a continuous liquid thread, (ii) a stable jet, where the jet forms a continuous liquid column without any bending or twisting, and (iii) a coiling jet, the state in which the jet rotates, bends, and folds periodically, forming a liquid-rope pile below the jet tail. The dependence of jet states on the applied voltage at different dispensing heights is summarized in three representative state diagrams for r_{top}/r_{bottom} and take values of 0.08, 0.25, and 0.42 [Figs. 2(b)–2(d)]. For instance, in Fig. 2(c), we observe that at a small dispensing height, as the voltage increases from 0 to 17 kV, a dripping jet becomes straight due to the stretching effect of the electrostatic stress, and no coiling is observed [type I in Fig. 2(e)]. For a dispensing height above h_c, the jet first drips at small voltage, then coils at a higher voltage, and

finally becomes a straight jet [type II in Fig. 2(e)]. The two types are characterized by the critical height h_c [red lines in Figs. 2(b)–2(d)], which is defined as the height above which a jet will coil at sufficient voltage and below which the jet would not coil under any practical applied voltage.

IV. DISCUSSION

A. Influence of the electric field on the slenderness of the jet

At the surface of the jet, the induced charge density can be estimated as $q_i \sim \varepsilon_1\varepsilon_0 E_n$, where ε_1 is the relative permittivity of the liquid and ε_0 is the vacuum dielectric constant. Thus, the normal and tangential electric stress exerted on the jet interface are $F_n^e \sim \varepsilon_1\varepsilon_0 E_n^2$, $F_t^e \sim \varepsilon_1\varepsilon_0 E_n E_t$, respectively [41]. We use the angle φ to denote the angle between the tangential of the jet surface and the electric field line at the point of investigation, as shown in Fig. 3(d). Then the normal electric force per unit area becomes $F_n^e \sim \varepsilon_1\varepsilon_0 E^2 \sin^2\varphi$ on the jet surface. The curvature of the jet surface influences the charge distribution along the jet [42]. The electric field strength and direction also vary with electrode configurations, implying a sophisticated force distribution. Though the exact charge distribution, the shape of the jet, and the electric stress are complicated to calculate in this configuration, we perform a force balance for an infinitesimal element on the surface of the jet at equilibrium. The jet forms a straight liquid thread at equilibrium and the force balance in the normal direction of the jet surface requires the normal electric stress to be balanced by a change of Laplace pressure [43] (see Sec. IV of the Supplemental Material [40] for schematic). We have the Laplace pressure of $\Delta P = F_e$, and since $\Delta P \sim \Delta[-(\gamma/a)]$, we obtain

$$\frac{\gamma}{a^2} da \sim \varepsilon_1\varepsilon_0 E^2 \sin^2\varphi,$$

where a is the local jet diameter and γ is the surface tension. From this expression, the jet expansion induced by the electric field is related to the electric capillary number [44], defined as $\mathrm{Ca}_e \equiv \varepsilon_1\varepsilon_0 E^2 a/\gamma$, which characterizes the ratio of electric stress and surface tension. Using $\delta = da/a$ as the shrinkage ratio, we obtain $\delta \sim \mathrm{Ca}_e \sin^2\varphi$. The expression shows that when φ decreases, the shrinkage ratio becomes smaller and the jet becomes wider. In our setup, when $r_{\mathrm{top}}/r_{\mathrm{bottom}}$ increases, the angle φ becomes smaller along the jet, as shown by the simulations reported in Figs. 3(a)–3(c) (see Supplemental Material [40] for simulation under different dielectric constant), and so does the radial electric force that balances the Laplace pressure. A small Laplace pressure implies a wider jet diameter, which has a smaller mean surface curvature. The experimental results shown in Fig. 3(e) performed with a fixed jet of length L and a constant voltage U also confirm that when the top electrode gets larger, the jet slenderness (a/L) gets larger (see Supplemental Material Sec. VI, part B for the method of calculating jet slenderness [40]). Therefore, the jet morphology is significantly affected by the electric field profile.

B. Onset of coiling influenced by jet slenderness

The jet morphology is a critical parameter for the onset of coiling, which can be reflected by one of the two key parameters that dominate the onset of coiling, (i) the slenderness $\xi = a/L$ and (ii) the compression force of the jet [21,45,46]. The viscous compressive stress acts as the buckling force while surface tension effects tend to minimize the jet surface area by stretching the filament toward both ends of the jet. The capillary number $\mathrm{Ca} = \mu V/\gamma$, which denotes the ratio of viscous to capillary forces, characterizes the compression strength on the jet. The gravitational effect is neglected here for $\rho g L/2 < 2\gamma/D$ [46]. The state diagram of coiling and noncoiling jets is summarized

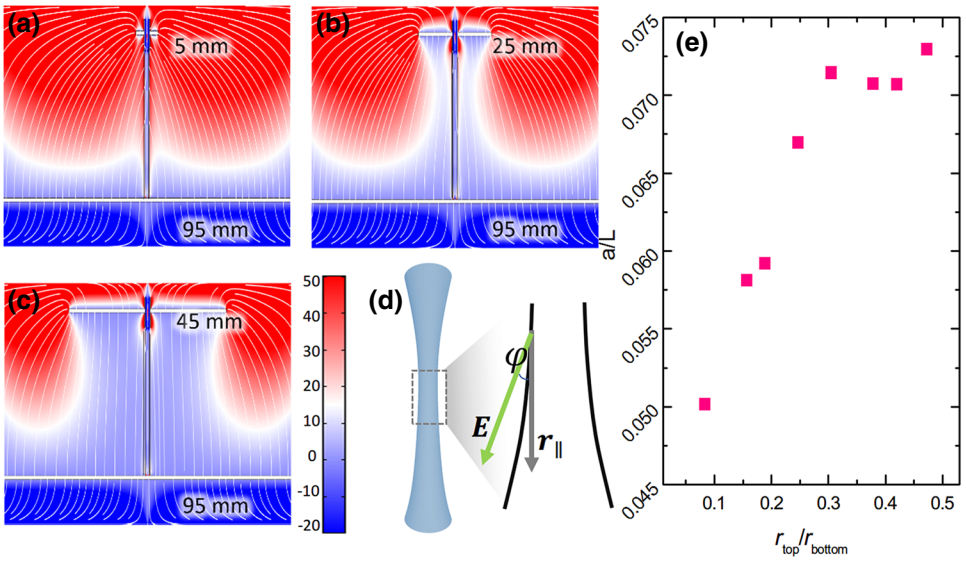

FIG. 3. Simulation results of the angle of the electric field to the surface of the jet and the slenderness of the jet under different electrode setup. The electric field direction around the jet when employing top electrode with a diameter of (a) 5 mm, (b) 25 mm, and (c) 45 mm. (d) The angle φ represents the angle of direction of the electric field with respect to the jet surface. Color scale in (a)–(c) denotes the value of the angle. (d) Experimental result of mean jet slenderness under different sizes of electrodes. The dispensing height and voltage are fixed at 13 mm and 5 kV, respectively.

by two dimensionless numbers: Ca, the capillary number and $\xi = a/L$, the jet slenderness, as shown in Fig. 4(a). Coiling only occurs for jets with a sufficiently strong compression and small slenderness. If the jet is slenderer, the compression needed is also smaller.

Now we take the applied electric force into force balance analysis, the electric force per unit length scales as $F_e = \varepsilon_0\varepsilon_1 E^2 r$, the surface tension force per unit length scales as $F_s = (\gamma/r)r$, and the viscous force scales as $F_v = \mu r^4 v/R^4$, where r is the radius of the thinnest part of the jet ($\sim$O(10^{-1}) mm), μ is the dynamic viscosity (approximately 20 Pa·s), v is the velocity of jet, and the radius of curvature of the coiling R is typically about O(1) mm. Therefore, the surface tension and the electric forces are comparable in magnitude, while the viscous force is smaller by four orders of magnitude. Thus, we define an electric capillary number $\mathrm{Ca}_e \equiv \varepsilon_0\varepsilon_1 E_n^2 a/\gamma$ that characterizes the ratio of the two dominating forces, as shown in Fig. 4(b).

We find that a larger top electrode will result in a wider jet, leading to larger values of the slenderness ξ. Since the flow rate does not change, a wider jet implies a smaller jet velocity, and in return leads to smaller compression. Both factors act against the onset of coiling, which can only occur when the jet is sufficiently slender and is subjected to a large axial compression. When the electrode configuration adopts a more conical shape, such as $r_{\mathrm{top}}/r_{\mathrm{bottom}} < 0.3$ in Fig. 2(a), the normal electric stress that points outward is effectively larger than those with larger top electrodes, thus requiring a larger Laplace pressure to balance; consequently, the jet diameter gets smaller. To satisfy mass conservation, the slenderness provides a larger speed to the jet and thus it hits the substrate and decelerates more rapidly, leading to larger compression as well. Thus, the critical height for coiling is smaller. A jet under a larger top electrode [$r_{\mathrm{top}}/r_{\mathrm{bottom}} > 0.3$ in Fig. 2(a)] will only coil when the height is sufficiently large to allow adequate thinning and compression of the jet.

C. Application in printing

Based on our understanding of the tunability of the electric field profile on the dynamical behaviors of the electrified jet, we propose a new tool for programming the printing of line patterns by changing the electrode configuration. A coiling jet extruded from a dispensing nozzle on a translational substrate draws various intricate patterns associated with different moving speeds and coiling frequencies [16,18,20,47–49]. We select two electrode configurations, one with a small top-plate electrode of $r_{\mathrm{top}}/r_{\mathrm{bottom}} \sim 0.08$, and the other with a larger top electrode of $r_{\mathrm{top}}/r_{\mathrm{bottom}} \sim 0.30$ [Fig. 5(a)], and set the dispensing height to a certain value. When the electric field is turned off, regardless of the electrode setup, the jet will spontaneously coil under the certain height, a value between the critical heights of the two configurations when the electric field is on. Therefore, when the same voltage is applied, the former jet manifests electric coiling [Fig. 5(b)], while the latter jet becomes straight and stable [Fig. 5(c)], in accordance with their respective positions in the state diagram in Fig. 5(a). We install a moving substrate to this setup, and each coiling rotation of the jet generates an air bubble in the deposited liquid thread shown schematically in Fig. 5(d), and a faster coiling generates denser bubbles. Thus, a plate-to-plate electrode configuration can suppress the coiling of jets and generate a straight liquid thread on

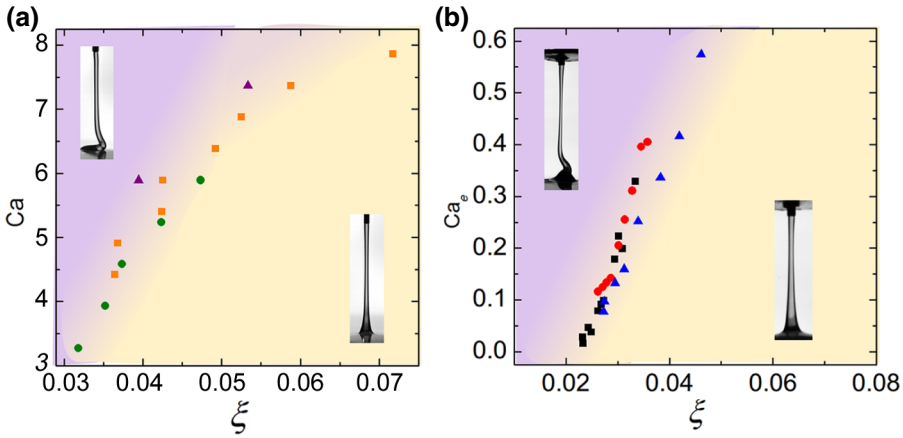

FIG. 4. The Ca $-$ ξ diagram for natural spontaneous coiling and Ca_e $-$ ξ diagram for electric coiling. Ca is the capillary number, Ca_e is the electric capillary number, and $\xi = a/L$ is the slenderness of the jet. The purple region represents the coiling and the yellow region represents the stable jet regime. (a) Diagram for coiling without electric field. The green, orange, and purple symbols correspond to lecithin, silicon oil of viscosity 60,000 and 10,000 cSt, and their flow rates are 5–12 ml/h for lecithin, 9–17 ml/h for 10,000 cSt silicone oil, and 2–3 ml/h for 60,000 cSt silicone oil, respectively. (b) Diagram for electric coiling. The blue, red, and black symbols represent no plate, 5.5 mm plate, and 8 mm aluminum plate as top electrode using lecithin, respectively.

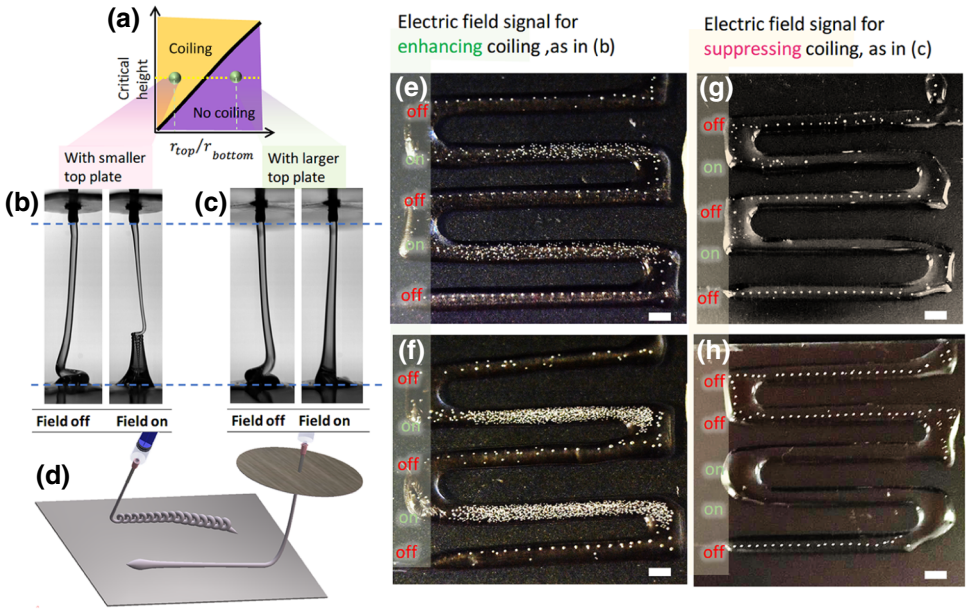

FIG. 5. The printed polycaprolacton (PCL)ink with different electrode configuration. (a) Diagram illustrating the coiling and no coiling regime with lecithin as the demonstrating fluid. (b) Side view of coiling of lecithin under smaller top plate. When the field is off, spontaneous coiling is observed. When the field is on, since the critical height is smaller than the current dispensing height, it can manifest electric coiling. Adopting this regime into printing, (e) and (f) demonstrate coiling with natural frequency, indicated by sparse bubbles when the field is off, and coiling with higher frequency, resulting in denser bubbles when the field is on. (c) With a larger top electrode, the dispensing height is smaller than the critical height where no electric coiling can be triggered regardless of the voltage. (g) and (h) shows the coiling phenomenon being suppressed when field is on and a straight line without bubbles is generated, while sparse bubbles are generated because of spontaneous coiling with the field off. (d) Schematic of the printed PCL-chloroform solution with a moving substrate. The scale bars are 5 mm. The flow rate is 15 ml/h.

demand by switching on the field, as shown in Figs. 5(e) and 5(g). Because in this case, the critical height is larger than the dispensing height, no coiling will be observed when the electric field is applied. While dense bubbles are needed, such as in forming a porous or multicavity material, we use a small-top electrode setup with critical heights smaller than the dispensing height. Thus, when the field is on, many more bubbles appear than natural coiling, as shown in Figs. 5(f) and 5(h). Not only can this method control when and where the bubbles appear or not, but it can also manipulate the density of the bubbles according to the moving speed of the plate and applied voltage. Specifically, when the tunable range of the dispensing height is restricted and a natural coiling is inevitable, a setup with large $r_{\text{top}}/r_{\text{bottom}}$ can suppress the natural coiling and avoid any bubbles if unwanted.

V. CONCLUSION

In this work, we identify and investigate the distinct role of the electric field profile on the onset of electric field-assisted liquid-rope coiling with various electrode configurations described by $r_{\text{top}}/r_{\text{bottom}}$. We use a critical height h_c above which the jet could exhibit a rope coiling effect upon an increase in voltage to characterize the jet behavior. Specifically, the larger the ratio $r_{\text{top}}/r_{\text{bottom}}$ is, which implies a more parallel field distribution, the larger the h_c is. The morphology of the jet is determined by balancing the normal electric stress and Laplace pressure on the jet surface at equilibrium. The relative strength of normal electric stress become smaller as $r_{\text{top}}/r_{\text{bottom}}$ gets larger, and the jet in turn becomes wider due to the reduction of Laplace pressure that balances the electric stress. As such, the jet gets wider as the electrode configuration goes from tip-to-plate to plate-to-plate, to reach a critical slenderness that supports a coiling and the critical height increases accordingly. In this manner, the onset height is tuned by varying the electrode configuration correspondingly. Our finding succeeds in accounting for the dynamic jet behaviors under different electrode configurations that a simplified model of uniform electric field distribution cannot. By manipulating the electrode configuration, printing and switching patterns with a desired density of bubbles on demand is realized by controlling the on and off state of the electric field. Specifically, our method realizes the suppression of natural coiling with a large value of $r_{\text{top}}/r_{\text{bottom}}$, a feature not possible with a bare-needle setup and simplified model. Our work enriches the physical picture of electric coiling and provides a promising alternative in printing porous scaffolds for bioengineering with a controllable

degree of porosity and in suppressing undesired formation of bubbles for fluid dispensing applications. It also provides a conceptual understanding for controlling electrified jets in fluid dispensing processes.

ACKNOWLEDGMENTS

This work was supported by the General Research Fund (Grants No. 17306315, No. 17304514, No, 17304017, and No. 17329516) from the Research Grants Council of Hong Kong, the General Program (Grant No. 21476189/B060201) and the Major Research Plan (Grant No. 91434202) from the National Natural Science Foundation of China as well as the Seed Fund for Basic Research (Grants No. 201711159249, No. 201611159205, and No. 201511159280), Seed Fund for Translational and Applied Research (Grant No. 201711160016) and Platform Technology Funding from the University of Hong Kong.

[1] G. I. Taylor, Electrically driven jets, Proc. R. Soc. Lond. A **313**, 453 (1969).
[2] Y. Huang, N. Bu, Y. Duan, Y. Pan, H. Liu, Z. Yin, and Y. Xiong, Electrohydrodynamic direct-writing, Nanoscale **5**, 12007 (2013).
[3] M. S. Onses, E. Sutanto, P. M. Ferreira, A. G. Alleyne, and J. A. Rogers, Mechanisms, capabilities, and applications of high-resolution electrohydrodynamic jet printing, Small **11**, 4237 (2015).
[4] Y. Duan, Y. Huang, Z. Yin, N. Bu, and W. Dong, Non-wrinkled, highly stretchable piezoelectric devices by electrohydrodynamic direct-writing, Nanoscale **6**, 3289 (2014).
[5] J. Feng, The stretching of an electrified non-Newtonian jet: A model for electrospinning, Phys. Fluids **14**, 3912 (2002).
[6] J. R. Melcher and W. J. Schwarz Jr, Interfacial relaxation overstability in a tangential electric field, Phys. Fluids **11**, 2604 (1968).
[7] S. Sankaran and D. Saville, Experiments on the stability of a liquid bridge in an axial electric field, Phys. Fluids A: Fluid Dyn. **5**, 1081 (1993).
[8] D. Saville, Electrohydrodynamic stability: fluid cylinders in longitudinal electric fields, Phys. Fluids **13**, 2987 (1970).
[9] D. H. Reneker and A. L. Yarin, Electrospinning jets and polymer nanofibers, Polymer **49**, 2387 (2008).
[10] T. Kong, J. Li, Z. Liu, Z. Zhou, P. H. Y. Ng, L. Wang, and H. C. Shum, Rapid mixing of viscous liquids by electrical coiling, Sci. Rep. **6**, 19606 (2016).
[11] T. Kong, H. A. Stone, L. Wang, and H. C. Shum, Dynamic regimes of electrified liquid filaments, Proc. Natl. Acad. Sci. U.S.A. **115**, 6159 (2018).
[12] B. Tchavdarov, A. Yarin, and S. Radev, Buckling of thin liquid jets, J. Fluid Mech. **253**, 593 (1993).
[13] N. M. Ribe, Coiling of viscous jets, Proc. R. Soc. Lond. A: Math. Phys. Eng. Sci. **460**, 3223 (2004).
[14] M. Habibi, S. Hosseini, M. Khatami, and N. Ribe, Liquid supercoiling, Phys. Fluids **26**, 024101 (2014).
[15] M. Maleki, M. Habibi, R. Golestanian, N. Ribe, and D. Bonn, Liquid Rope Coiling on a Solid Surface, Phys. Rev. Lett. **93**, 214502 (2004).
[16] M. Habibi, Y. Rahmani, D. Bonn, and N. Ribe, Buckling of Liquid Columns, Phys. Rev. Lett. **104**, 074301 (2010).
[17] S. Chiu-Webster and J. Lister, The fall of a viscous thread onto a moving surface: A 'fluid-mechanical sewing machine', J. Fluid Mech. **569**, 89 (2006).
[18] R. Passieux, L. Guthrie, S. H. Rad, M. Lévesque, D. Therriault, and F. P. Gosselin, Instability-assisted direct writing of microstructured fibers featuring sacrificial bonds, Adv. Mater. **27**, 3676 (2015).
[19] J. I. Lipton and H. Lipson, 3D printing variable stiffness foams using viscous thread instability, Sci. Rep. **6**, 29996 (2016).
[20] W.-m. Yang, T.-k. Zhu, Y.-a. Jin, and J.-z. Fu, Facile fabrication of helical microfluidic channel based on rope coiling effect, Microsyst. Technol. **23**, 2957 (2017).
[21] N. M. Ribe, M. Habibi, and D. Bonn, Liquid rope coiling, Annu. Rev. Fluid Mech. **44**, 249 (2012).
[22] M. Habibi, M. Maleki, R. Golestanian, N. M. Ribe, and D. Bonn, Dynamics of liquid rope coiling, Phys. Rev. E **74**, 066306 (2006).
[23] J. O. Cruickshank, Dissertation (1980).
[24] H.-Y. Kim, M. Lee, K. J. Park, S. Kim, and L. Mahadevan, Nanopottery: Coiling of electrospun polymer nanofibers, Nano Lett. **10**, 2138 (2010).
[25] N. Bhardwaj and S. C. Kundu, Electrospinning: a fascinating fiber fabrication technique, Biotechnol. Adv. **28**, 325 (2010).
[26] T. Han, D. H. Reneker, and A. L. Yarin, Buckling of jets in electrospinning, Polymer **48**, 6064 (2007).
[27] Z.-M. Huang, Y.-Z. Zhang, M. Kotaki, and S. Ramakrishna, A review on polymer nanofibers by electrospinning and their applications in nanocomposites, Compos. Sci. Technol. **63**, 2223 (2003).
[28] L. Y. Yeo, Z. Gagnon, and H.-C. Chang, AC electrospray biomaterials synthesis, Biomaterials **26**, 6122 (2005).
[29] B. Almería and A. Gomez, Electrospray synthesis of monodisperse polymer particles in a broad (60 nm–2 μm) diameter range: Guiding principles and formulation recipes, J. Colloid Interface Sci. **417**, 121 (2014).
[30] A. D. Duong, G. Ruan, K. Mahajan, J. O. Winter, and B. E. Wyslouzil, Scalable, semicontinuous production of micelles encapsulating nanoparticles via electrospray, Langmuir **30**, 3939 (2014).
[31] M. Cloupeau and B. Prunet-Foch, Electrostatic spraying of liquids in cone-jet mode, J. Electrostat. **22**, 135 (1989).
[32] H. F. Poon, *Electrohydrodynamic printing* (2002).
[33] J. Schneider, N. Lindblad, C. Hendricks Jr, and J. Crowley, Stability of an electrified liquid jet, J. Appl. Phys. **38**, 2599 (1967).
[34] J. Feng, Stretching of a straight electrically charged viscoelastic jet, J. Nonnewton. Fluid Mech. **116**, 55 (2003).
[35] L. Konermann, E. Ahadi, A. D. Rodriguez, and S. Vahidi, (ACS Publications, 2012).
[36] P. Juhasz, M. G. Ikonomou, A. T. Blades, and P. Kebarle, in *Methods and Mechanisms for Producing Ions from Large Molecules* (Springer, 1991), pp. 171.

[37] L. A. B. Pilkington, Review lecture. the float glass process, Proc. R. Soc. Lond. A: Math. Phys. Sci. **314**, 1 (1969).

[38] C. E. Stauffer, The measurement of surface tension by the pendant drop technique, J. Phys. Chem. **69**, 1933 (1965).

[39] D. Saville, Electrohydrodynamics: The Taylor-Melcher leaky dielectric model, Annu. Rev. Fluid Mech. **29**, 27 (1997).

[40] See Supplemental Material at http://link.aps.org/supplemental/10.1103/PhysRevApplied.12.014034 for more simulations, plots of other parameters, extra experimental results, and more setup details.

[41] I. Hayati, A. Bailey, and T. F. Tadros, Mechanism of stable jet formation in electrohydrodynamic atomization, Nature **319**, 41 (1986).

[42] C. Burcham and D. Saville, Electrohydrodynamic stability: Taylor–Melcher theory for a liquid bridge suspended in a dielectric gas, J. Fluid Mech. **452**, 163 (2002).

[43] T. Kong, Z. Liu, L. Wang, and H. C. Shum, Suppressing the Folding of Flowing Viscous Jets Using an Electric Field, Phys. Rev. Appl. **3**, 034010 (2015).

[44] A. R. Thiam, N. Bremond, and J. Bibette, Breaking of an Emulsion Under an ac Electric Field, Phys. Rev. Lett. **102**, 188304 (2009).

[45] J. Cruickshank and B. R. Munson, Viscous fluid buckling of plane and axisymmetric jets, J. Fluid Mech. **113**, 221 (1981).

[46] M. Le Merrer, D. Quéré, and C. Clanet, Buckling of Viscous Filaments of a Fluid Under Compression Stresses, Phys. Rev. Lett. **109**, 064502 (2012).

[47] N. M. Ribe, J. R. Lister, and S. Chiu-Webster, Stability of a dragged viscous thread: Onset of "stitching" in a fluid-mechanical "sewing machine", Phys. Fluids **18**, 124105 (2006).

[48] Y. Yu, F. Fu, L. Shang, Y. Cheng, Z. Gu, and Y. Zhao, Bioinspired helical microfibers from microfluidics, Adv. Mater. **29**, 1605765 (2017).

[49] P.-T. Brun, B. Audoly, N. M. Ribe, T. S. Eaves, and J. R. Lister, Liquid Ropes: A Geometrical Model for Thin Viscous Jet Instabilities, Phys. Rev. Lett. **114**, 174501 (2015).